# EFFECT OF THE SEA SURFACE ROUGHNESS ON LIDAR RETURN CHARACTERISTICS

**B.A. Kargin, G.M. Krekov, and M.M Krekova**

*Computing Center,*
*Siberian Branch of the Russian Academy of Sciences, Novosibirsk*
*Institute of Atmospheric Optics,*
*Siberian Branch of the Russian Academy of Sciences, Tomsk*
*Received December 17, 1991*

*Mean energy and power of a return signal of an airborne lidar operating at* $\lambda = 0.5$ μm *under conditions of the wind–driven sea waves are estimated by the Monte Carlo method. Their dependence on the wind velocity varying in the range* $1 \le V \le 7$ m/s, *on the optical conditions, and on the experimental geometry is studied. The formation of lidar return received from the underwater is shown to be primarily determined by the sea surface state.*

A run of experiments on laser aerosounding of the upper layer of the ocean has shown its promise not only for direct express high–precision bathymetry of coastal waters but also for solving a wide range of problems related to monitoring and studying the sea water composition. Laser sounding of the upper layer of the ocean allows the data to be obtained on behavior of optical parameters.

Quantitative and qualitative characteristics of the reflected signal are determined by the experimental geometry, stratification of optical properties of sea water (SW), and the state of the air–water interface. Some papers, for example, Refs. 1 and 2, pointed out the need to take into account the sea surface roughness when interpreting the lidar return because of the revealed correlation between the absolute level of the signal and the state of sea roughness.

The problem of charting the waters in accordance with optical properties or depth stratification of optical properties assumes retrieving quantitative information from the lidar return. The requirements for the reliability of the obtained data have brought about the need for the theoretical study of the effect of different factors, including the roughness of the sea surface, on peculiarities of temporal shaping of the recorded signal.

This paper presents the results of numerical simulation intended for studying the specific nature of shaping of the lidar return under conditions of wind–driven waves. Possible signal focusing observed in several cases[1,3] has been theoretically treated earlier, for example, in Ref. 4, and is not considered here.

The power and energy of lidar return can be found by solving a nonstationary radiative transfer equation with the initial and boundary conditions which are typical of the airborne monostatic lidar operation. The estimates are performed by the Monte Carlo method which allows one to separately analyze the reflected signal shape as a function of variations in the optical parameters of the medium and of the experimental geometry.

Having solved the problem, we find the estimates of average (over space or over an ensenible of realizations) radiation energy and power recoded by the receiving system.

Without dwelling on theory and algorithms for solving such problems described elsewhere[5] in detail, we will briefly deal only with some points of mathematical formulation of the problem.

In this paper we examine the layer $0 \le z \le H$ of a three–dimensional uniform space filled with light scattering and absorbing matter. Within the layer, at the altitude $z = h$, there is an interface between two media: atmosphere and ocean, which is represented as ingomogeneous surface comprising a set of randomly oriented facets whose centers lie in the plane $z = h$ while $\mathbf{S} = (S_x, X_y, S_z)$ are the normals to these facets.

The transport of photons in the medium is regulated by prescribing the scattering phase function $g(\mu)$ and the extinction σ, scattering $\sigma_s$, and absorption $\sigma_a$ coefficients.

The plane $z = 0$ is the bottom being the Lambertian reflector with the albedo $A_L$. The source, located at the altitude $z = \{x_s, y_s, z_s\}$ is assumed to emit instantaneously $(\delta(t - t_0))$ a light signal whose energy is distributed isotropically within the solid angle $\Omega_s$ with divergence angler $\varphi_s$. A diffusely reflected signal is recorded by the receiver located at $r_r = (0, 0, z_r)$ within the solid angle $\Omega_r$ with the angle of the receiver field of view $\varphi_r$.

The problem is to estimate the energy and temporal shape of lidar return.

The Monte Carlo method is employed for solving the radiative transfer equation written for convenience in the integral form

$$I(\mathbf{r}, \mathbf{w}, t) = S(\mathbf{r} - \xi_0\boldsymbol{\omega}) \exp\left\{ -\int_0^{\xi_0} \sigma(\mathbf{r} - \xi'\boldsymbol{\omega})\, d\xi' \right\} +$$

$$+ \frac{1}{2\pi} \int_0^{\xi_0} d\xi \sigma_s(\mathbf{r} - \xi\boldsymbol{\omega}) \exp\left\{ -\int_0^{\xi_0} \sigma(\mathbf{r} - \xi'\boldsymbol{\omega})\, d\xi' \right\} \times$$

$$\times \int_\Omega d\omega' g(\mathbf{r} - \xi\boldsymbol{\omega}, \mu)\, I(\mathbf{r} - \xi\boldsymbol{\omega}, \boldsymbol{\omega}', t) . \qquad (1)$$

Here $I(\mathbf{r}, \boldsymbol{\omega}, t)$ is the total intensity of radiation at the point $\mathbf{r}$ in the direction $\boldsymbol{\omega}$ and $\mu = (\boldsymbol{\omega}, \boldsymbol{\omega}')$. The function $S(\mathbf{r}, \boldsymbol{\omega})$ is determined by the distribution of sources and by the effect of the medium interface on the radiation

$$S(\mathbf{r}, \boldsymbol{\omega}) = \begin{cases} I_0 |\boldsymbol{\omega}| , \ \boldsymbol{\omega} \in \Omega_- , \ z = z_s , \\ I(\mathbf{r}, \boldsymbol{\omega}) , \ \boldsymbol{\omega} \in \Omega , \ z = h , \\ I(\mathbf{r}, \boldsymbol{\omega}) , \ \boldsymbol{\omega} \in \Omega_+ , \ z = 0 , \end{cases} \qquad (2)$$

0235-6880/92/03 191-05 $02.00 

where

$$I(\mathbf{r}, \omega)\,|_{\omega \in \Omega_+,\, z=0} = \dot{R}_0 I\,,$$

$$I(\mathbf{r}, \omega)\,|_{\xi \in \Omega_+,\, z=h} = \dot{R}_h I\,,$$

$$\xi_0 = \begin{cases} (z-H)/c\,,\ z \in [h, H]\,,\ \omega \in \Omega_-\,, \\ (z-h)/c\,,\ z \in [h, H]\,,\ \omega \in \mathrm{W}_+ \\ \text{and } z \in [0, H]\,,\ \omega \in \Omega_+\,, \\ z/c,\ z \in [0, h]\,,\ \omega \in \Omega_-\,, \end{cases} \qquad (3)$$

where $\Omega_+$ is the hemisphere with $c \in [-1, 0]$, $\Omega$ is the hemisphere with $c \in [0, 1]$, $\Omega$ is a set of all directions $[-1, 1]$, $\dot{R}$ is the linear integral operator describing the law of radiation reflection from the plane $z = 0$, and the operator $\dot{R}_h$ describes the effect of the air–water interface on radiation is written in the form[6]

$$\dot{R}_h I = \int\limits_{\Omega_+} \mathrm{d}S \int\limits_{\Omega} P(\mathbf{S})\, R(\omega', \mathbf{S})\, I((\mathbf{r}_\perp, h), \omega')\delta(\omega' - \omega_s)\, \mathrm{d}\omega' +$$

$$+\nu^2 \int\limits_{\Omega_+} \mathrm{d}S \int\limits_{\Omega} P(\mathbf{S})\,(1 - R(\omega', \mathbf{S}))\, I((\mathbf{r}_\perp, h), \omega')\, \mathrm{d}(\omega' - \omega_r)\, \mathrm{d}\omega', \quad (4)$$

where $R(\omega', \mathbf{S})$ is the Fresnel reflectance, $\mathbf{S}$ is the external normal to the facet, $P(\mathbf{S})$ is the probability density of the normals.[6] Starting from the representation of the surface as a set of randomly oriented facets on the basis of the results given in Ref. 6, we assume that the normals to the facets obey the truncated two–dimensional probability density of slopes $z_x$ and $z_y$

$$P(\mathbf{S}) = P(z_x, \mathbf{z}_y) = 2\pi(\sigma_x\sigma_y)^{-1} \exp\left\{-(z_x/\sigma_x)^2/2 - (z_x/\sigma_x)^2/2\right\}, \quad (5)$$

where $z_x = S_x/S_z$, $z_y = S_y/S_z$, and the slope variances change as a function of wind velocity as

$$\sigma_x^2 = 0.00316\ V\ ;\ \sigma_y^2 = 0.003 + 0.00192\ V\ . \qquad (6)$$

Note that Pelevin[7] pointed based on the measurements in the Black Sea, on the one hand, that the applicability of the empirical model is limited by the surface wind velocity $V \le 7$ m/s, and proposed the wind velocity dependences of $\sigma_x^2$ and $\sigma_y^2$ in the form

$$\sigma_x^2 = 0.00174 + 0.00157V \text{ and } \sigma_y^2 = 0.00134 + 0.0012V. \quad (7)$$

On the other hand, a run of experimental measurements carried out for wind velocities $7 < V < 15$ m/s showed a good agreement between the empirical and normal distributions.

When solving the problems of laser sensing the use of the facetted model is justified for the description of the sea roughness state. Indeed, it was shown in Ref. 9 that the choice of a model for calculating a portion of reflected radiation is unimportant for the radiation incident on the surface at the angles $0 < 0 < 60°$ with respect to the vertical. In particular, the calculations made in Ref. 9 for two more general facetted models of the sea roughness gave practically the same results. The optical model of roughness must be refined at glancing angles of sounding when shading of waves and rereflection of radiation between them are observed. Relations (6) and (7) were employed as a model describing the behavior of variances of the facet slopes as a function of the wind velocity.

As is well known, the algorithms for statistical simulation of lidar systems with localized detectors are based on the so–called local estimate of the flux. If an arbitrary point of scattering is in the atmosphere, then local estimate has the form (see, e. g. , Ref. 10):

$$\varphi(\omega_j,\ \mathbf{r}_j \to \omega,\ \mathbf{r}_r) = \frac{\exp(-\tau(\mathbf{r}_j\ \mathbf{r}_r))\ g(\mu)}{2\pi|\mathbf{r}_j - \mathbf{r}_r|^2}\ \Delta(\Omega_r)\ \Delta_i\ t\ , \qquad (8)$$

where $\Delta(\Omega_\rho)$ is the indicator of the region $\Omega_r$, $\Delta_i t$ is the characteristic function of the $i$th time interval, $\tau(\mathbf{r}_j, \mathbf{r}_r)$ is the optical thickness of the atmosphere between the points $\mathbf{r}_j$ and $\mathbf{r}_r$ in the direction $\omega = \dfrac{\mathbf{r}_r - \mathbf{r}_j}{|\mathbf{r}_r - \mathbf{r}_j|}$, and $\mu = (\omega_j, \omega)$. When the point of collision is at the interface, the form of estimate (8) holds, but the scattering phase function $g(\mu)/2\pi$ is replaced by the probability density of the chosen facet slope $P(\mathbf{S})$ and the reflectance $R(\omega_j, \mathbf{S})$ is taken into account.

For the collisional points being in a water medium, it is expedient to replace the unconditional kernel of transition (8) $\varphi(\omega_j, \mathbf{r}_j \to \omega, \mathbf{r}_r)$ by the product of the conditional transition and the probability of the condition

$$\varphi(\omega_j, \mathbf{r}_j \to \omega, \mathbf{r}_r) = \varphi(\omega_j, \mathbf{r}_j \to \mathbf{S}, \mathbf{r}' \to \omega, \mathbf{r}_r)\, P(\mathbf{S})(1 - R(\omega'_j, \mathbf{S}))/n^2.$$

The calculated results given below were obtained for a monostatic lidar operating at $\lambda = 0.5$ μm and located in the atmosphere at a distance $z_r = 200$ m from the interface. The optical axis of lidar was oriented in the nadir, the angular divergence of the source $\varphi_s = 2'$ and the angle of the receiver field of view varied in the limits $2' \le \varphi_r \le 2°$. The optical properties of the atmosphere over the ocean were for the Deirmenjian's $M$ haze[11] and the extinction coefficient was $\sigma = 2$ km$^{-1}$ over the entire layer.

The light extinction coefficient in the sea water being the multicomponent medium was represented in the form

$$\sigma = \sigma_{aw} + \sigma_{sw} = \sigma_{sh} + \kappa_{ch}C_{ch} + \kappa_{ym}C_{ym}\ ,$$

where $\sigma_{aw}$, $\sigma_{sw}$, and $\sigma_{sh}$ are the coefficients of absorption and scattering by clear water and by suspended undissolved particles of organic and mineral origin, $\kappa_{ch}$ and $\kappa_{ym}$ are the absorptivities of chlorophyll and yellow matter, and $C_{ch}$ and $C_{ym}$ are their concentrations.

Following the recommendations given in Ref. 12, we take the following values of the aforementioned parameters: $\sigma_{aw} = 0.0271$ m$^{-1}$, $\sigma_{sw} = 0.0023$ m$^{-1}$, $\kappa_{ch} = 0.025$ m$^2$/mg, $\kappa_{ym} = 0.022$ m$^{-1}$, $C_{ch} = 0.5$ mg/m$^3$, and $C_{ym} = 0.5$. Two types of scattering phase functions were employed in calculations[13]: $g_1(\mu)$ with its mean cosine $\langle\cos\mu\rangle = 0.95$ and $g_2(\mu)$ for which $\langle\cos\mu\rangle = 0.8$. Moreover, in the directions near 180° the values of $g_2(\mu)$ are almost an order of magnitude higher than that of $g_1(\mu)$. The scattering phase functions of the first type $g_1(\mu)$ are typical of the open ocean, and those of the second type $g_2(\mu)$ are typical of

coastal water with enhanced concentration of mineral fraction. The calculations were performed for wind velocities varying between 1 and 7 m/s, i.e., in the absence of foam formed on the sea surface due to breaking of waves.

Taking into account the possible losses of that portion of radiation which is reflected from the rough surface, we first consider the effect of wind–driven waves on variations in the level of radiation energy entering the detector.

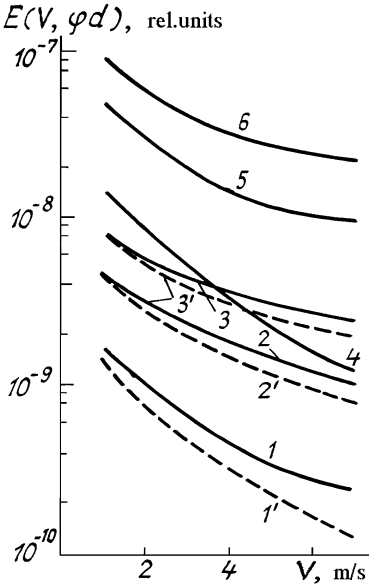


*FIG. 1. Wind velocity dependence of the average lidar return energy. Curves 1 – 3 are for $E_I(V)$, 1′–3′ are for $E_{II}(V)$, calculation with the scattering phase function $g_1(\mu)$; 4 – 6 are for $E_{II}(V)$, calculation with $g_2(\mu)$; curves 1, 1′, and 4; 2, 2′, and 5; 3, 3′, and 6 are for $1/2\varphi_r$ = 2′, 12′, and 40′, respectively;* $\sigma = 0.2$ m$^{-1}$ *and* $W = 0.823$.

Figure 1 shows the dependences of the average energy $E(V, \varphi_d)$ calculated, respectively, for relations (6) describing model I and (7) describing model II determining the relation of the facet slope variances to the wind velocity. The results of calculations show that the average energy decreases with increase of the sea roughness within the entire above–indicated range of reception angles. Increase in the beam divergence due to spread in the directions of photons that cross the randomly oriented facets results in the fact that some photons leave the receiver field of view and the total level of signal decreases. The choice of the wind velocity dependence of $\sigma_x^2$ and $\sigma_y^2$, when estimating $E$, is unimportant for $V < 1.5$ m/s. The discrepancies in the estimates $E_I$ and $E_{II}$ grow with increase of the wind velocity, they are particularly important for small reception angles ($\varphi_r \sim \varphi_s$) and become practically the same at large reception angles.

Shown in Fig. 1 are curves *1–3* and *4–6* calculated using the scattering phase functions $g_1(\mu)$ and $g_2(\mu)$, respectively. They show that in both cases the $V$–dependence of the average energy $E$ has the same qualitative character, only the absolute levels of signal energe are different.

The comparison between the average lidar return energy under conditions of wind–driven sea waves and the signal calculated for a flat interface is shown in Fig. 2. The losses in energy due to the roughness can reach 50–90% depending on the viewing cone. As the results of calculations show the changes in the extinction coefficient $\sigma$ and in the probabilities of photon servival $W$ result in variations in the absolute level of the energy $E$ but qualitative dependence of $E(V)$ holds. Indeed, the calculations of the ratio $E/E_{aw}$ (shown in Fig. 2) carried out for $\sigma = 0.4$ m$^{-1}$ and $W = 0.9$ as well as for 0.1 and $W = 0.6$ reveal its insignificant qualitative and quantitative variations.

Retrieval of the optical properties of sea water is often based on the single–scattering approximation. The character of formation of the average singly scattered signal energy $E_1$ changes together with the total signal energy under conditions of the wind–driven sea waves.

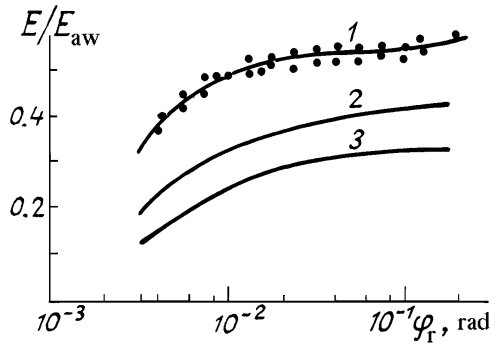


*FIG. 2. Ratio of the energy of return signal of the lidar operating under conditions of the wind–driven sea waves to that in the absence of waves as a function of the field of view of the detector and of the wind velocity. Curves 1–3 are for* $V = 3$, 5 *and* 7 m/s; *dots are for* $\sigma = 0.4$ *and* 0.1 m$^{-1}$, $V = 3$ m/s.

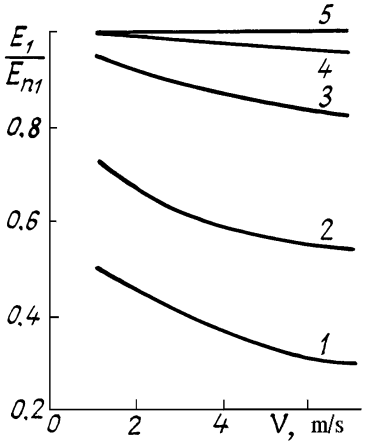


*FIG. 3. The dependence of the ratio $E_1/E_{1n}$ on the angular dimensions of the receiver curves 1–5 are for $1/2\varphi_r$ = 2′, 12′, 20′, 30′, and 1°, calculation with the scattering phase function $g_1(\mu)$,* $\sigma = 0.2$ m$^{-1}$ *and* $W = 0.823$.

As can be seen from the numerical estimates, the level $E_1$ depends on the angles of the receiver field of view. It increases with $\tilde{\varphi}_r$ and reaches the maximum level $E_{1n}$. Further it remains unchanged for any $\varphi_r > \tilde{\varphi}_r$. Figure 3 shows the ratio of the average energy of a singly scattered signal $E_1$ entering the given receiving aperture to the maximum value of the average energy of singly scattered signal $E_{1n}$ as a function of the wind velocity. In the above–considered example, $E_{1n}$ is reached for

the angle $\varphi_r \sim 30' - 1°$. For a flat interface, the singly scattered signal in the experimental geometry under consideration is concentrated in the angle $\varphi_r \simeq \varphi_s$. Based on the estimates the maximum level $E_{1n}$ reaches not more than 70% of the energy of the singly scattered signal calculated for a plane–stratified medium. The calculated results show that under the effect of wind–driven waves the decrease of the total level of the average lidar return energy for the limited aperture is strongly accounted for by the decrease of the absolute level of the energy of signals of lowest–order scattering. The relative contribution of $E_1$ to $E$ is given in Table I.

*TABLE I. The dependence of the ratio $E_1/E$ (%) on the angular dimensions of the detector $\varphi_r$ and on the wind velocity.*

| $V$, m/s | Scattering phase function | | | | | | | |
|---|---|---|---|---|---|---|---|---|
| | $g_1$ | | | | $g_2$ | | | |
| | $\varphi_d$, grad | | | | | | | |
| | 2′ | 12′ | 40′ | 2° | 2′ | 12′ | 40′ | 2° |
| 1 | 90 | 82 | 64 | 35 | 85 | 68 | 53 | 28 |
| 3 | 89 | 79 | 62 | 33 | 81 | 64 | 51 | 28 |
| 5 | 88 | 70 | 56 | 28 | 78 | 58 | 51 | 27 |
| 7 | 87 | 63 | 50 | 26 | 75 | 56 | 26 | 26 |

At wide receiving apertures the dependence of $E_1/E$ on the wind velocity disappears, in particular, for the medium characterized by a less elongated scattering phase function.

Thus the lidar operation under conditions of the wind–driven sea waves is accompanied by significant losses of the lidar return energy which are particularly high at small angles of the receiver field of view $\varphi_r \sim \varphi_s$. As the calculations show, the most optimal from the standpoint of reduction of the energy losses, are the apertures $\varphi_r \gtrsim 10\ \varphi_s$.

Before proceeding to the analysis of peculiarities in the formation of the temporal shape of lidar return, we are concerned with its distribution over the multiplicities of interaction. Figure 4 shows the power of the singly scattered signal $p^{(1)}(h)$ as a function of the depth of the layer being sounded and the angular dimensions of the receiving aperture. A qualitative character of the $p^{(1)}(h)$ behavior changes with increase of the angle $\varphi_r$, its formation runs to completion when $\varphi_r \sim 30' - 1°$.

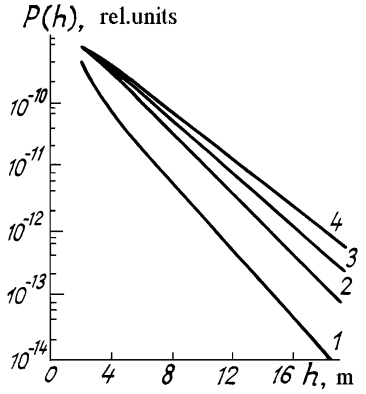


*FIG. 4. The temporal dependence of the singly scattered signal power calculated for the wind velocity $V$ = 3 m/s: curves 1–4 are for $1/2\varphi_r$ = 2′, 12′, 20′, and 40′, $\sigma$ = 0.2 m$^{-1}$, $W$ = 0.823, and $\sigma_x$ and $\sigma_y$ distribution I given by Eq. (6).*

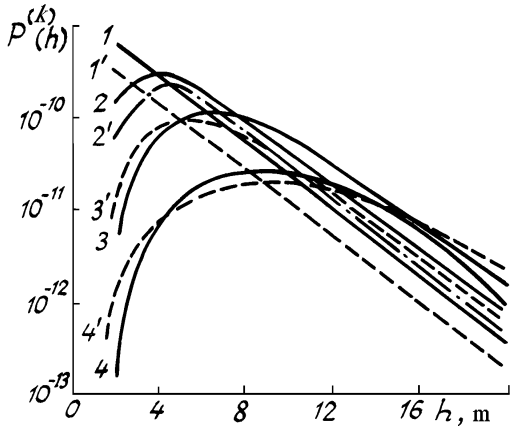


*FIG. 5. The signal power distribution over multiplicities of interaction. The numbers of the curves correspond to the order of scattering. Curves 1–4 are for $V$ = 1 m/s and curves 1′–4′ are for $V$ = 3 m/s; $1/2\varphi_r$ = 40′.*

Under conditions of wind–driven sea waves the broadening of angular dimensions of the beam due to the photons that intersect twice the irregular interface, causes transformations of the signal shape first of all due to radiation of lowest–order scattering. Shown in Fig. 5 is the average lidar return power distribution over multiplicities of scattering $P^{(k)}(h)$ for two values of wind velocity. The decrease in the power levels of the first two multiplicities of scattering is observed with increase of $V$. The levels $P^{(k)}(h)$ of the orders of scattering $k > 2$ depend, to a smaller extent, on variations in the wind velocity. Nevertheless, as compared with a flat interface,[14] the changes in the character of formation of higher–order scattering are observed. The monotonic increase in powers of $p^{(k)}(h)$ is found to occur when $k > 2$, their maxima are broad, and no sharp decay is observed. Such a behavior of $p^{(k)}(h)$ for $k > 2$ is apparently provided by photons which during their interaction with the interface or particles of the medium leave the receiver field of view but from the periphery enter the receiver after repeated intersection of the facets of the surface. The calculations made with the scattering phase functions $g_1(\mu)$ and $g_2(\mu)$ show that when the asymmetry of $g(\mu)$ decreases, the maxima in $p^{(k)}(h)$ of multiplicities $k > 2$ undergo additional broadening.

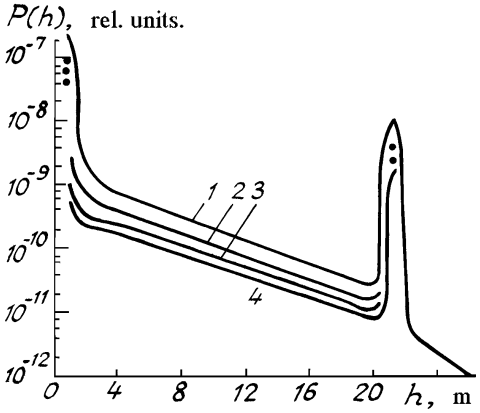


*FIG. 6. Transformation of the temporal shape of the signal as a function of wind velocity: curves 1–4 are for $V$ = 1, 3, 5, and 7 m/s, $1/2\varphi_r$ = 40′, $\sigma$ = 0.2 m, $W$ = 0.813, and $A_L$ = 0.2.*

The wind velocity dependence of the total lidar return power $P(h)$ is shown in Fig. 6. The increase in wind velocity is accompanied by the decrease of the absolute level of power $P(h)$. At first the differences between the levels of $P(h, V)$ are most pronounced. Further they come closer. The signal coming from the deeper sounded layers is weakly affected by variations in the wind velocity since it is primarily formed by the photons with highest orders of scattering whose $V$–dependence (see Fig. 5) is less pronounced.

It should be noted in conclusion that during the bathymetric measurements the effect of wind–driven sea waves does not hinder seriously recording of the signal reflected from the bottom (see Fig. 6). Only the absolute level of the signal decreases while its relative level remains sufficiently high.

## REFERENCES

1. F. Hoge and R. Swift, Appl. Opt. **22**, No. 1, 37 (1983).
2. D.V. Vlasov, Izv. Akad. Nauk SSSR, ser. Fizika **49,** No. 5, 433 (1985).
3. F. Hoge and R. Swift, Appl. Opt. **22**, No. 23, 3778 (1983).
4. V.N. Vlasov, V.N Strel'tsov, and V.A. Slobodyanin, in: *Trudy IOFAN* (Nauka, Moscow, 1986), Vol. 1, p. 39.
5. E.O. Dzhetybaev and B.A. Kargin, in: *Current Problems of Applied Mathematics and Numerical Simulation* (Nauka, Novosibirsk, 1982), p. 83.
6. C. Cox and W. Munk, J. Opt. Soc. Am. **44**, No. 11, 838 (1954).
7. V.N. Pelevin, in: *Ocean Optics* (Nauka, Moscow, 1983), Vol. 2, p. 101.
8. V.F. Tsyplukhin and L.M. Martsinkevich, Izv. Akad. Nauk SSSR, ser. Fiz. Atmos. Okeana **9,** No. 7, 748, (1973).
9. S.M. Prigarin, Cand. Phys.–Math. Sci. Diss., Computating Center of the Siberian Branch of the Russian Academy of Sciences, Novosibirsk (1990).
10. G.I. Marchuk, et al., *The Monte Carlo Method in Atmospheric Optics* (Springer, Berlin, 1980).
11. D. Deirmendjian, *Electromagnetic Scattering on Spherical Polydispersions* (Elsevier, Amsterdam; American Elsevier, New York, 1969).
12. O.V. Kopelevich and K.S. Shifrin, in: *Optics of the Ocean and Atmosphere* (Nauka, Moscow, 1981), p. 4.
13. G.M. Krekov and M.M. Krekova, Atm. Opt. **2**, No. 1, 55 (1989).
14. G.M. Krekov, M.M Krekova, and I.V. Samokhvalov, Issled. Zemli iz Kosmosa, No. 6, 77, (1986).